

EBBINNOT: A Hardware Efficient Hybrid Event-Frame Tracker for Stationary Neuromorphic Vision Sensors

Deepak Singla , Member, IEEE, Vivek Mohan , Member, IEEE, Tarun Pulluri , Andres Ussa ,
Bharath Ramesh , Member, IEEE and Arindam Basu , Senior Member, IEEE

Abstract—In this paper, we present a hybrid event-frame approach for detecting and tracking objects recorded by a stationary neuromorphic vision sensor (NVS) used in the application of traffic monitoring. To enable long-term, battery powered usage in IoT, we propose a hardware efficient processing pipeline that optimizes memory and computational needs. The usage of NVS gives the advantage of rejecting background while it has a unique disadvantage of fragmented objects due to lack of events generated by smooth areas such as glass windows. To exploit the background removal, we propose an event based binary image (EBBI) creation that signals presence or absence of events in a frame duration. This reduces memory requirement and enables usage of simple algorithms like median filtering and connected component labeling (CCL) for denoise and region proposal (RP) respectively. To overcome the fragmentation issue, a YOLO inspired neural network based detector and classifier (NNDC) to merge fragmented region proposals has been proposed. Finally, a simplified version of Kalman filter, termed overlap based tracker (OT), exploiting overlap between detections and tracks is proposed with heuristics to overcome occlusion.

The proposed pipeline is evaluated using more than 5 hours of traffic recording spanning three different locations. Our proposed hybrid architecture outperformed (AUC = 0.45) Deep learning (DL) based tracker SiamMask (AUC = 0.33) operating on simultaneously recorded RGB frames while requiring $2200\times$ less computations. Compared to pure event based mean shift (AUC = 0.31), our approach requires $68\times$ more computations but provides much better performance. Finally, we also evaluated our performance on two different NVS: DAVIS and CeleX and demonstrated similar gains. To the best of our knowledge, this is the first report where an NVS based solution is directly compared to other simultaneously recorded frame based method and shows tremendous promise by outperforming DL based solutions on frames.

Index Terms—Neuromorphic vision, Event based sensor, Region Proposal, Neural Network, Tracking, Low-power

List of Abbreviations- NVS: Neuromorphic Vision Sensor, IoT: Internet of Things, DL: Deep Learning, EBBI: Event-based Binary Image, COTS: Commercial off-the shelf, KF: Kalman Filter, NN-Filter: Nearest Neighbor Filter, OT: Overlap based Tracker, EBMS: Event based Mean Shift, RP: Region Proposal, AER: Address Event Representation, HIST: Histogram, CCL: Connected Component Labeling, ANN: Artificial Neural Network, CNN: Convolutional Neural Network, VOT: Visual Object Tracking, 1B1C: 1-bit 1-channel image, 1B2C: 1-bit 2-channel image, SC: Superior Colliculus, BB: Bounding Box, NNDC: Neural Network Detector plus Classifier, GT: Ground Truth, IoU: Intersection-over-Union, AUC: Area under Curve, NMS: Non-maximal Suppression, FOV: Field-of-view

D. Singla, V. Mohan and A. Basu are with the School of EEE, Nanyang Technological University, Singapore

T. Pulluri, A. Ussa, and B. Ramesh are with the N.I Institute for Health, National University of Singapore, Singapore

I. INTRODUCTION

Neuromorphic vision sensors (NVS) operating on a retina-inspired principle provide advantages of ideal sampling due to change detection driven sensing, low data rates, high dynamic range and high effective frame rate [1]–[3]. It has largely been touted to be useful for high speed tracking due to microsecond resolution of events [4]–[8]. However, many practical applications from the field of internet of things (IoT) such as traffic monitoring do not require very high speed of tracking—rather, it is more important to reduce false positives. Additionally, event driven tracking requires very stringent denoise operations to reduce false positives—often found to be quite difficult to achieve. While NVS does reduce the data rate, it is also necessary to develop a full processing pipeline of low complexity operators that can result in energy efficient hardware for deployment in IoT. Current event-based processing algorithms often require a significant amount of memory and processing due to noise related events. Finally, no real comparisons are available so far in comparing an NVS with a regular image sensor on the same application. With the massive growth in Deep learning (DL) based visual solutions, it is essential to ask the question of how well does an NVS perform in object detection and tracking as compared to regular cameras with their output processed by DL algorithms.

In this work, we show that in applications such as traffic monitoring with stationary NVS, the change detection property of NVS can enable high accuracy detection and tracking when combined with simple DL techniques of much less complexity than conventional ones [9]. In particular, we propose a new processing pipeline for stationary neuromorphic cameras that involve:

- A novel hybrid approach of creating event-based binary image (EBBI) involving time collapsing and intensity quantization of event stream. This also enables duty cycled operation of the NVS making it compatible with commercial off-the shelf (COTS) hardware such as microcontroller units (MCU) and FPGA for IoT that rely on duty cycling for reducing energy.
- The use of simple frame-based filtering techniques for denoising the EBBI, with noise suppression comparable to conventional event-based noise filtering approaches such as NN-filter [10]. These denoised EBBI frames require lower memory, making them suitable for implementation while simplifying the detection and tracking components

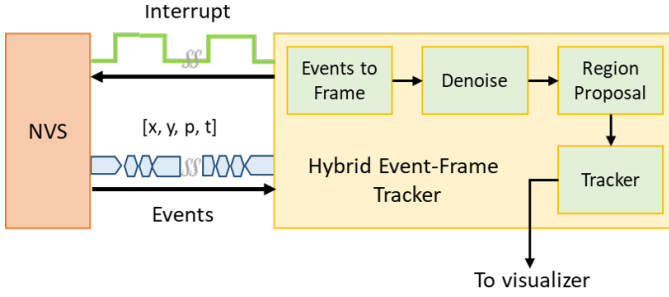


Fig. 1: Generalized block diagram for EBBINNOT

in the proposed pipeline.

- Superior colliculus (SC) inspired high accuracy object localization and region proposal, implementing connected component analysis on spatially down-sampled, low-resolution images.
- A hybrid neural network based detector-classifier (NNDC) flow for merging fragmented object bounding boxes and object aware false positive suppression caused by EBBI frame generation. The NNDC rectified bounding boxes can then be fed to a tracker.
- The overlap based tracker (OT) which is a computationally less intensive simplification of traditional Kalman Filter (KF) for EBBI, combining rule-based heuristics with KF like prediction and correction approach.

Since our proposed solution combines EBBI, NN based region proposal and OT for tracking, we refer to it as EBBINNOT. Figure 1 shows a block diagram of EBBINNOT depicting the major blocks in the processing pipeline as well as the possibility of duty cycled interface with a NVS. It is to be noted that such hybrid approaches are becoming popular recently [11] and supporting hardware solutions are also being released [12]. An earlier version of this work was presented in [13]—however, the histogram region proposal used in [13] suffered from inaccurately sized and fragmented regions.

The rest of the paper is organized as follows: the next section reviews some of the background information about NVS and tracking algorithms. Section III describes the proposed algorithms in EBBINNOT and their computational complexities compared to conventional ones. Section IV presents the performance of each block as well as the whole pipeline and compares them with relevant baselines such as histogram based region proposal (HIST RP), Kalman filter (KF) based tracking, pure event based mean shift (EBMS) tracking and pure RGB frames followed by DL based tracking. This is followed by a section that discusses the main results and also shows that our approach is NVS independent and yields expected results with two commercially available NVS: DAVIS [14] and CeleX [15]. Finally, we conclude in the last section.

II. BACKGROUND

A. Neuromorphic Vision Sensor (NVS)

A NVS or event camera, unlike a traditional image sensor with fixed frame rate, operates by detecting temporal contrast (or change in log-intensity) at all pixels in parallel. If the change is larger than a threshold, it generates an asynchronous digital pulse or spike or event with a timestamp and a pixel

location associated to it. Further, a polarity is assigned to each and every event according to the direction (increase or decrease) of contrast variation. This type of signalling is referred to as address event representation (AER). These changes in the format of data produced hence require a paradigm shift in the algorithms required for processing the input for various applications, opening up a whole new avenue in engineering [1], [3].

Mathematically, an event can be modeled as $[e_i = (x_i, y_i, t_i, p_i)]$ where (x_i, y_i) represents the event location or address on the sensor array, t_i represents the timestamp of the event and p_i represents the polarity associated to it [16]. The associated timestamps to each event have microsecond resolution with quick readout rates ranging from 2 MHz to 1200 MHz. The event camera has an in-built invariance to illumination, since it detects temporal contrast change largely cancelling out the effect of scene illumination. In short, the variation in log intensity represents the variation in reflectance due to the movement of the objects in the view.

B. Tracking

Visual tracking is a fundamental operation in video processing [17], and is critically needed in applications ranging from autonomous vehicles to traffic surveillance. For event driven NVS, one can perform tracking either directly on events or generate frames (at fixed time interval or at fixed event counts [18]) to apply conventional frame driven techniques. We next review classical examples of three such algorithms.

1) *Kalman Filter based Tracking*: A classical application of Kalman Filter (KF) in computer vision involves estimating the position of a detected object in a two-step process - prediction of object position and correction to refine the estimates considering noise measurements [19]. Object tracking using KF (KF Tracker) as implemented in [20], associates detections to the track of the same object by estimating the track's location in each frame, and determining the likelihood of assignment of tracks and detections using Hungarian Assignment. Unassigned detections seed a new track and a count of visibility of all tracks is maintained to delete tracks which may have left the scene, when it remains invisible beyond a certain number of frames. Estimating the number of computations performed per frame and the memory required to track objects is an important step to assess the suitability of a tracker for power and area constrained applications such as remote surveillance. Since our proposed OT method in Section III is closely related to KF, we detail the derivation of the number of computations per frame, C_{KF} (based on [21], [22]), for KF Tracker as follows:

$$\begin{aligned}
 C_{KF} &= N_T(C_p + P_a C_c + P_{uat} C_u + C_{cost}) \\
 &\quad + N_{obj}(P_{ua} C_{new}) + C_{ha} \\
 C_p &= 4m^3 + 3m^2 + 2mn \\
 C_c &= 6m^3 + 6m^2n + 2mn^2 + 3m^2 + 7mn + m + n \\
 C_u &= 2, C_{new} = 1 \\
 C_{cost} &= 4n^3 + 2m^2n + 2mn^2 + 5n^2 + 5 \\
 C_{ha} &= 1/6(11N_{obj}^3 + 12N_{obj}^2 + 31N_{obj}) \quad (1)
 \end{aligned}$$

where N_T and N_{obj} are the average number of tracks and objects per frame respectively, P_a is the probability of assignment of detection to track, P_{ua} and P_{uat} are the probabilities of unassigned detection and track respectively, and m , n are the sizes of state and measurement vectors respectively. C_p , C_c , C_u , C_{ha} , C_{cost} , C_{new} in eq. 1 represent the average number of computations per frame involved in the logic for prediction, correction, track update, Hungarian assignment, cost estimation of assignment of detection/track and seeding a new track respectively. Likewise, based on [23], we define the memory requirements for KF per frame, M_{KF} , as follows:

$$M_{KF} = N_T \times WS(5m^2 + m(3n + 1) + n^2 + 2n) + (A \times B) \quad (2)$$

where, $A \times B$ is the dimension of a binary frame and WS is the word size. Then, assuming $A = 240$, $B = 180$, $WS = 32$ and $N_T = 8$, the estimated storage needed would be approximately 6.8KB.

2) *Event based Mean Shift (EBMS) Tracking*: This is a representative algorithm that operates directly on events with a good computational performance. The mean shift tracking approach used on frames in early 2000s [24] was modified for application on event clusters in [7]. These event clusters represent the moving objects with each having events occurring in close proximities. The new cluster positions and velocities are modeled with the help of mixed equation of old positions and velocities and the new incoming event location. The cluster is considered active only if it contains a threshold number of events, and is lost if no new events are found inside it for a threshold period. This method is advantageous since the events occur only at few pixels and the majority of the scene is unchanged.

3) *Deep learning based Tracking*: For standard RGB frames, Bromley *et al.* [25] demonstrated first success after using Siamese inspired artificial neural network (ANN) architecture to verify signatures. In general, Siamese architecture resembles the physical structure of conjoined twins. Following the significant progress in ANNs, these architectures turned out to be efficient for image matching and verification using one-shot learning [26]. With the development of deep convolutional neural networks (CNNs) and availability of large data sets for training, fully convolutional Siamese (SiamFC) networks [27] turned out to be efficient online tracking architectures using similarity matching.

SiamMask [28] is inspired from the great success of SiamFC for object tracking. Unlike traditional CNNs, it solely relies on initial bounding box coordinates of the target in the first frame of the video stream, which is referred to as an *exemplar image*, and estimates object position to generate segmentation mask in subsequent images. SiamMask works on the principle of similarity matching between an exemplar image and a search image. To initialize this tracking process for the n^{th} frame, we provide ground truth information for the object-of-interest, i.e. exemplar image, and the subsequent $(n+1)^{th}$ frame is treated as the search image.

Based on the above input, SiamMask generates an object mask and its corresponding anchor box by max-min techniques



Fig. 2: SiamMask tracking a vehicle, mask generated is denoted by red colour and corresponding anchor box calculated using max-min method in green colour

[28] on the search image, as shown in Figure 2. This current anchor box information along with the $(n+1)^{th}$ frame is used as the exemplar image to track the object-of-interest in the $(n+2)^{th}$ frame. This process continues and objects are tracked for rest of the sequence. However, SiamMask fails to track in case of missing object-of-interest [28]. To avoid such scenarios, only search images with object-of-interest are made to be part of the test sequence. By avoiding such scenario, we are also eliminating false positives which indeed provide the best-case scenario for SiamMask in our evaluation.

Apart from establishing itself as the state-of-the-art on the popular visual object tracking (VOT 2018) benchmark, SiamMask is also popular for its simplicity, speed and online learning. Thus, we compare the proposed NVS object tracking pipeline with SiamMask, applied to simultaneously recorded RGB frames for a close comparison.

III. MATERIALS AND METHODS

The proposed EBBINNOT system comprises of three major blocks (Fig. 3): EBBI and noise filtering, region proposal network (RPN) and tracking described in details below.

A. Event Data Pre-processing

1) *Event Based Frame Generation*: In this work, we propose to aggregate events occurring within a specified time-interval (denoted by t_F for frame time) into two types of temporally collapsed images. First, a *single channel binary image* (1-bit, 1-channel image denoted as 1B1C in Fig. 3) was created by considering a pixel to be activated i.e., $I(x_i, y_i) = 1$ for any event mapping to the pixel location (x_i, y_i) and $I(x_j, y_j) = 0$ for any pixel (x_j, y_j) with no activity within the interval, irrespective of the polarity of the event and the event count for that pixel location. Second, a *dual channel binary image* (1-bit, 2-channel image denoted as 1B2C in Fig. 3) was obtained in the same way as in case of 1B1C, with the exception that events corresponding to two polarities are written separately, with one channel consisting of ON events and the other consisting of OFF events. Note that 1B1C can be obtained by logical OR of the two 1B2C images—however, in practice, it is better to create the two images simultaneously to avoid further delays due to memory access.

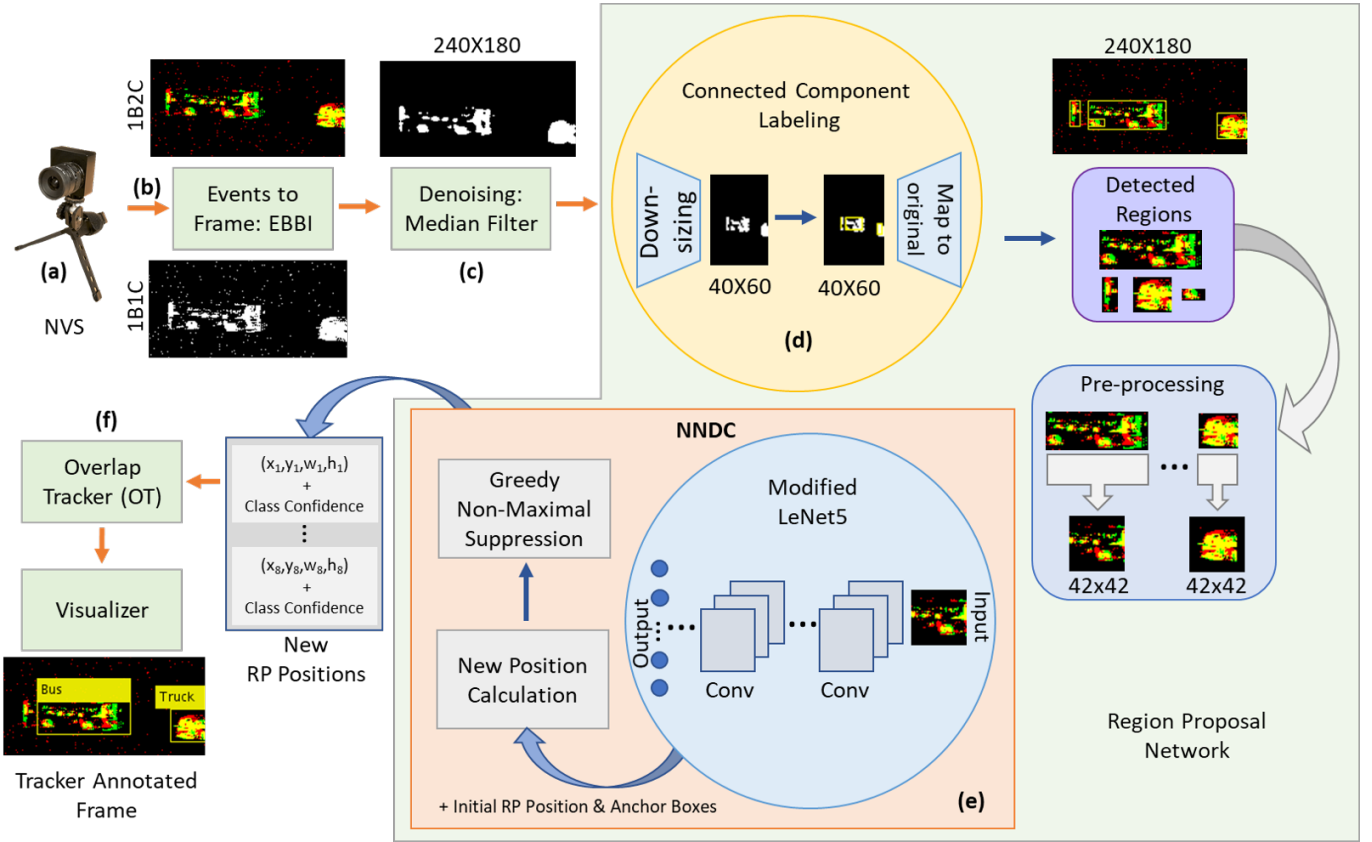


Fig. 3: Detailed block diagram of the EBBINNOT pipeline for 240×180 sensor like DAVIS. For larger sensor like CeleX, the image was downsampled appropriately by dropping lower address bits of the events, thus mapping multiple sensor pixels to same image location. Input events from the (a) NVS is converted to a binary image in (b) EBBI module (ON and OFF events in 1B2C is shown by two different colours) followed by (c) median filtering for noise removal. The region proposal (RP) consists of (d) connected component labelling and (e) NNDC blocks. The last block is the (f) tracker

Note that this is different from the downsampling methods in [29] where the total number of events in frame duration is counted to create a multi-bit image which has been shown to be not as informative as 1B2C for classification [30]. Event count based images may be thresholded to arrive at these EBBIs which have advantage of being hardware friendly and amenable to processing via application of simple morphological operators [31]. Akin to how visual information exits the occipital lobe into two distinct visual systems composed of *what* and *where* pathways [32], in our work, the region proposal network for locating the object is comparable to the *where* pathway. Finally, this proposed method of EBBI allows the processor (Fig. 1) to be duty cycled since it need not count all events within the time t_F —rather, the NVS can act as a memory and retain the addresses of all events triggered in the interval till the processor wakes up, reads and resets it. Other methods of frame generation such as [18], [33] relying on fixed event count, are unsuitable when there are multiple objects in the frame with varying sizes. Lastly, we use $t_F = 66$ ms in this work, but have seen the general concept works for a range of t_F varying from 30–120 ms. Even lower values of t_F might be needed for tracking faster objects at the expense of power dissipation, while going to $t_F > 120$ ms led to very high motion blur in our application.

2) *Noise Filtering*: A conventional event-based filtering for an event stream from the NVS as presented in [10], [34], involves a combination of refractory filtering to minimize high frequency noise characterized by abnormal firing rates due to leakages in some of the pixel sensors, followed by an event-based nearest neighbouring filter (NN-Filter) which passes events occurring within a specified time interval in the neighbourhood of the event. For events in an $A \times B$ sensor dimension, represented by B_t bits per timestamp, a $p \times p$ NN-Filter, performs p^2-1 counter increments and comparisons besides a memory write for B_t bits. The total computes and memory required when NN-Filtering is performed for an average of \bar{n} events per frame was obtained as follows in [13]:

$$\begin{aligned} C_{NN-Filter} &= (2(p^2-1) + B_t) \times \bar{n} \\ M_{NN-Filter} &= B_t \times A \times B \end{aligned} \quad (3)$$

Note that $\bar{n} = \beta \times \alpha \times A \times B$ where $\beta (> 1)$ denotes the average number of times a pixel fires in duration t_F and α is the number of active pixels in the frame.

The creation of EBBI enables us to leverage the use of median filter, a standard image processing tool, which ensures noise removal by replacing a pixel with the median value in its $p \times p$ neighborhood, while preserving the object edges [31]. For removal of spurious noise due to pixel firing which roughly

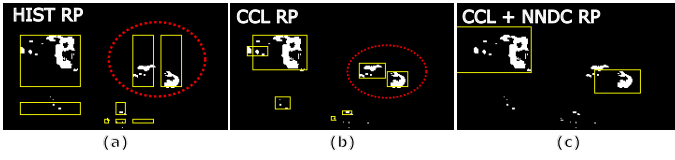


Fig. 4: Comparison of different region proposal methods: (a) HIST RP presents the problem of enlarged and fragmented bounding box due to the presence of bigger object, (b) CCL RP resolves the inaccurate bounding box issue posed by (a) however object bounding box fragmentation is still observed, (c) CCL+NNDC RP resolves fragmentation problem and removes unwanted bounding boxes

translates to salt and pepper type of noise in a 1B1C EBBI, a median filter performs an equivalent of p^2 counter increments for every 1 and $\lfloor p^2/2 \rfloor$ comparisons, besides memory writes for creating the filtered EBBI. The average number of computations per $A \times B$ frame using a median filter on an EBBI is given by:

$$\begin{aligned} C_{Median-Filter} &= (\alpha p^2 + 2) \times A \times B \\ M_{Median-Filter} &= 2 \times A \times B \end{aligned} \quad (4)$$

where the memory requirement is to store the raw and filtered 1B1C EBBI frames.

With a conservative estimate of objects covering $\alpha = 10\%$ of screen area and assuming $A = 240$, $B = 180$ for DAVIS sensor [14], we obtain $C_{NN-Filter} \approx 276.4$ Kops/frame and $C_{Median-Filter} = 125.2$ Kops/frame for $p = 3$. Further, the median filter approach requires nearly $8 \times$ lesser memory than a conventional NN-filter. Lastly, we show in Section IV that the performance of the EBBI with median filtering is at par with the much more expensive NN-Filter.

B. Region Proposal Networks

A crucial step to understand the visual scene involves the detection of salient visual cues, and the role of SC behind the natural vision [35], [36] is a perfect example for detection. Fundamentally, the natural vision pathway astounds researchers mostly because of its speed and efficiency, and SC proves efficient here by obtaining salient objects from a low spatial resolution version of the input [37]. Surprisingly, the low resolution achromatic images allows better performance and faster response due to less computes. Inspired by these, we propose to use a low-resolution version of 1B1C images in this work for the first phase of region proposal as described next.

1) *Move from HIST RP to CCL RP*: The projection of event information into EBBI and rejection of background by a stationary NVS provides us an opportunity to use well-known frame-based simple operators like edge detection and thresholding. To understand the context in the frame, learning the distribution of active pixels in an already foreground background separated EBBI is the key. Histogram based RP (HIST RP) explored in [13], [38], [39], extracts one-dimensional (1-D) X and Y histograms by summing up all the active pixels along the respective axis. These histogram distributions can then be easily analyzed and the consecutive entries higher

than some threshold can be used to locate the probable object locations back in 2-D.

However, operating this algorithm on the image at original sensor resolution can likely yield two or more areas for the fragmented images (e.g. glass windows in cars do not generate events and lead to fragmented clusters of events representing a car as shown in Fig. 4)(a) but an appropriately chosen down-scaled version of the same image merges most of the objects. Further, a second run to weed out the false regions is done by checking the presence of active pixels in the proposed regions from the previous step. These steps still cannot help overcome the shortcoming of projecting back from 1-D to 2-D where the box for the smaller object gets affected in the presence of a bigger object (shown in Fig. 4). A tight bounding box (BB) is required for a better understanding of the object in the classification stage.

Therefore, instead of using 1-D projections, we propose to use the morphological 2-D operator like connected component labeling (CCL RP). CCL RP relies on the connectivity of a target pixel with its surrounding eight pixels, called 8-connectivity neighbours. A two-pass algorithm of CCL reviewed in [40], [41] and proposed for operation on 1B1C EBBI in [30], produces tight BBs for an effective classification process. This algorithm relies on the equivalent label in the 8-connectivity neighborhood and continuously updates the BB corners of each and every pixel using the equivalent label during its two raster scans. Applied on a downsized version of EBBI for the same reason as HIST RP, this RP also keeps the computes in control. The downsizing is also a great example of exploration of low spatial resolution saliency detection aspect of the human visual system. The downsizing is done by scaling factors s_1 and s_2 as follows:

$$I^{s_1, s_2}(i, j) = \bigvee_{m=0, n=0}^{m=s_1-1, n=s_2-1} I(i s_1 + m, j s_2 + n) \quad i < \lfloor A/s_1 \rfloor, j < \lfloor B/s_2 \rfloor \quad (5)$$

where $I(i, j) \in \{0, 1\}$ and s_1, s_2 are rescaling factors along X and Y axis and \bigvee represents the logical-OR operation on a patch.

The computational and memory complexity of HIST RP are reported in [13]. The corresponding equations for CCL RP labeled as C_{CCL} and M_{CCL} as derived in eq. 6, depend on the parameter α since the main comparisons in the algorithm happen only on active pixels. The first term of $C_{CCL}(M_{CCL})$ denotes the contribution of downsizing. We can keep a fixed memory assuming that we have maximum number of equivalent labels, possible only when there is an inactive pixel between every two active pixels. Therefore, the second term in M_{CCL} indicates the memory required for storing the four BB corners for each equivalent label.

$$\begin{aligned} C_{CCL} &= A \times B + \alpha \frac{A \times B}{s_1 s_2} \\ M_{CCL} &= \frac{A \times B}{s_1 s_2} + \\ &\quad \left(\frac{A \times B}{2 s_1 s_2} \lceil \log_2 \left(\frac{A}{s_1} \right) \rceil + \frac{A \times B}{2 s_1 s_2} \lceil \log_2 \left(\frac{B}{s_2} \right) \rceil \right) \end{aligned} \quad (6)$$

For our specific case, we estimated α to be between 2.7 and 4.5, by running CCL RP over the dataset as discussed later in the paper. Combining that with the sensor dimensions for DAVIS camera $A = 240$, $B = 180$ and well fitting scaling factors $s_1 = 6$, $s_2 = 3$ for our case, we estimated that HIST RP performs $C_{HIST} = 48$ Kop/frame and $M_{HIST} = 3.44$ KB while CCL RP has maximum $C_{CCL} \approx 54$ Kop/frame ($\alpha = 4.5$) and $M_{CCL} = 16.8$ KB. Although, the number of computations are similar for both HIST and CCL RPs, the memory requirement increases five fold for CCL. However, it should be noted that such increase does not play much role in the system level since it is much less than the memory required by NNDC as shown in the following sub-section.

2) *Combining CCL and NNDC RP*: Although there are low-cost frame-based single step object detector and classifier solutions in the literature such as YOLO [9], [42], SSD-MobileNet [43], in order to target for stand-alone IoVT devices based real-time traffic monitoring, implementing such CNN based networks in compact, power-constrained hardware (< 1 mW) is not feasible.

CCL RP discussed earlier, plays a fundamental role in recognizing salient information from the achromatic binary image, but does not cover highly fragmented objects such as buses, trucks in some of the scenes generating more than two RPs for single objects (shown in Fig. 4(b)). Therefore, a secondary correction step for removing unwanted RPs and merging BBs is required. However it will require the knowledge about the RP and its associated class in order to merge them [42]. Keeping in mind the memory constraints, we propose a CNN based Detector (position correction) plus Classifier model (NNDC RP) which predicts the class and confidence for the RP, and correctly modifies the position of RP bounding box.

The initial inspiration for this model came from YOLOv2 [42] wherein, the idea of predicting BB coordinates offsets and usage of hand-picked anchor boxes (priors) was proposed. We borrow these ideas from YOLOv2 and apply them on a variant of LeNet5 [44], [45], with a $42 \times 42 \times 2$ input, cropped from the centroid or symmetrically zero-padded image from RP bounding box coordinates of 1B2C frame.

The network produces $C + 5$ outputs including confidences for all available classes (C), objectness score (BB_{conf}) and bounding box correction parameters (t_x, t_y, t_w, t_h). This model differs from YOLOv2 in the following aspects: (a) in place of the entire frame, the input to the model is RP obtained from CCL, (b) the anchor boxes are determined from mean sizes of class categories each representing one of the classes, unlike k-means clustering used in YOLOv2, and (c) the prediction contains just one bounding box per input RP instead of multiple bounding boxes for each grid cell of the input frame. The rest – hidden layers, activations, number of filters, filter sizes for convolution layers, in the modified model are kept the same, except for BB_{conf} and BB correction parameters which have linear activation. Physically, BB_{conf} represents whether the RP being analyzed contains sufficient information about the object or not, and a threshold (thr) to it helps in flagging the RP for rejection or consideration for passing to tracker. BB correction parameters (\hat{t}_x, \hat{t}_y) represent

the predicted offset for upper left corner (RP_x, RP_y) of RP bounding box, while (\hat{t}_w, \hat{t}_h) represent the predicted width and height correction parameters for the box’s width and height (RP_w, RP_h).

We note that predicting the offsets, (\hat{t}_x, \hat{t}_y) has a huge advantage and makes the training smoother [42]. However, learning the sizes of the objects is the most important aspect for the model and therefore, we feed the knowledge of priors to the model. We ensure that the number of priors are equal to the number of classes, C , with each prior corresponding to a class. The anchor box sizes are determined from the mean sizes of ground truth (GT) BBs for each of the classes in the input dataset. The new size of RP is predicted using the anchor box size of the predicted class and size correction parameters for the RP. The complete algorithm for the calculation of corrected RP location is shown in Algorithm 1.

Algorithm 1: New Position Calculation

Input : A list $[(w_i, h_i)], i = 1, 2, \dots, C$, where each tuple is anchor box size for class i .
A list $[\hat{o}_i], i = 1, 2, \dots, C$, where each element is predicted confidence for class i .
Bounding Box predicted correction parameters:
 $[\hat{B}B_{conf}, \hat{t}_x, \hat{t}_y, \hat{t}_w, \hat{t}_h]$
Initial location of RP’s top left corner:
 (RP_x, RP_y)

Output: New Region Proposal BB Location: $[\hat{x}, \hat{y}, \hat{w}, \hat{h}]$

if $BB_{conf} < thr$ **then**
| Box is rejected;
else
| find $j, \max(\hat{o}_j)$ where $j \in 1, 2, \dots, C$;
| for that j , get (w_j, h_j) ;
| $\hat{x} = clip(\tanh(\hat{t}_x) * (A - 1) + RP_x, 0, A - 1)$;
| $\hat{y} = clip(\tanh(\hat{t}_y) * (B - 1) + RP_y, 0, B - 1)$;
| $\hat{w} = clip(w_j * exp(\hat{t}_w), 0, A)$;
| $\hat{h} = clip(h_j * exp(\hat{t}_h), 0, B)$;
| where, $clip(a, m, n)$ means a is clipped with m as lower bound and n as upper bound
end

Model Training: While training the model, we gather all the RPs from all the training videos frame by frame and resize them into a fixed size of $42 \times 42 \times 2$, either by zero padding keeping the RP in centre or cropping it from the centroid. The true positions for each of the RPs for a particular frame are defined according to the intersection-over-union, IoU (eq. 7) with the ground truth (GT) bounding boxes for that frame. If the IoU of RP with GT box is greater than $IoU_{th} = 0.1$, the true BB_{conf} for that RP is assigned the same value as IoU and GT bounding box, $[x, y, w, h]$ act as true location for the RP; otherwise, BB_{conf} is kept 0.

$$IoU = \frac{A_{Intersection}}{A_{Union}} \quad (7)$$

where $A_{Intersection}$ is the area of intersection and A_{Union} is the area of union of RP box and the GT box. Therefore,

we form the new loss function (eq. 8) combining the three components given by:

$$\begin{aligned}
 Loss_1 &= \sum_{i=1}^C (o_i - \hat{o}_i)^2 \\
 Loss_2 &= (BB_{conf} - \hat{B}B_{conf})^2 \\
 &\text{if } BB_{conf} > 0.1, \\
 Loss_3 &= \left(\frac{x - \hat{x}}{A - 1}\right)^2 + \left(\frac{y - \hat{y}}{B - 1}\right)^2 + \left(\frac{w - \hat{w}}{A}\right)^2 + \left(\frac{h - \hat{h}}{B}\right)^2 \\
 &\text{else,} \\
 Loss_3 &= 0 \\
 \text{Total Loss} &= Loss_1 + Loss_2 + \lambda * Loss_3 \quad (8)
 \end{aligned}$$

where, λ is the Lagrange multiplier used to give appropriate weightage to the third component. It also helps the model to give attention to better position detection. This loss function is largely modified from YOLOv1 [46], with the penalization for BB coordinates being changed according to the *IoU* of RP box with the GT box, and the width and height of boxes optimized directly instead of their square roots.

While testing the model, the predicted $\hat{B}B_{conf}$ helps in rejecting the RPs and the new BB coordinates are predicted only if $\hat{B}B_{conf}$ is greater than the assigned threshold, IoU_{th} . Therefore, the knowledge of priors gives an upper-hand in predicting finely localized box and the corresponding class information. This object detector, however may be left with multiple overlapping boxes for the same object after prediction. Consequently, we suggest the application of three-step greedy non-maximal suppression (NMS) [47] for removing the unwanted overlapping boxes:

- Sort the new BBs for a particular frame according to the predicted $\hat{B}B_{conf}$.
- Start with the best scoring box and find its *IoU* with the other BBs one-by-one and suppress the other BB if *IoU* is greater than a fixed threshold, thr^{ms} .
- Repeat the same procedure with the next box in the sorted array until no extra boxes remain in the list.

It is to be pointed out that the calculation for rectified bounding box may seem unconstrained, however, the knowledge of RP being a part of the complete object allows the network to learn that the actual bounding box of required object is at a small offset of RP and has size as a factor of the prior class size. Further, this modified version of LeNet5 does not add much computes to the original model and performs much faster than other object detector models (shown in Table I). It can be seen that Tiny YOLOv2, YOLOLite and SSD-MobileNet have $\approx 52\times$, $\approx 24\times$, $\approx 16.8\times$ higher computes per frame respectively than this model. The computes and parameters for other models were calculated on an image size of $240 \times 180 \times 2$, which is the sensor dimensions of DAVIS with information in ON-OFF polarity channels. For NNDC, assuming a range of 1 – 8 RPs in the frame, total computes per frame for NNDC can vary from 2.16M to 17.25M. For a fair comparison with other models, we also combine the computes for EBBI and CCL RP leading to a total computes bound per frame of $\approx 17.302M$ for our proposed approach.

TABLE I: Computations for different object detector and classifier models

Network	Total # Computes	# Parameters
NNDC	2.16-17.3M	0.108M
Tiny YOLOv2 [42]	898M	15.74M
YOLOLite [48]	418M	0.542M
SSD-MobileNet [43]	290M	26.34M

Note that these two blocks do not add much computes to the overall total, showing that most of the computation is done in the neural network model.

C. Overlap based Tracking

Inspired by KF, we present a simpler tracker that takes advantage of two properties of stationary NVS: (a) rejection of background, and (b) very fast frame rates. Due to these two factors, the assignment of detections to tracks can be simplified to just checking overlap followed by greedy assignment, hence the name overlap based tracker (OT). Occlusion is handled by having extra checks based on predicted trajectories, assuming a constant velocity model. OT works on the principle of prediction of current tracker position from past measurements and correction based on inputs from the region proposal (RP) network [13]. Using P_i and T_i ($1 \leq i \leq 8$) to represent bounding boxes obtained from the region proposal network and OT respectively, each composed of upper-left corner coordinates (x,y) and object dimensions (w,h), the major steps performed by the OT for each EBBI frame, can be summarized as follows:

- 1) The tracker is initialized and the predicted position $T_i^{pred}(x, y)$ of all valid trackers is obtained by adding $T_i(x, y)$ with corresponding horizontal (V_x) and vertical (V_y) velocity.
- 2) For each valid tracker i in the *tracking* or *locked* mode, T_i^{pred} is matched with all available region proposals P_j . A match is found if overlapping area between the T_i^{pred} and P_j is larger than a certain fraction of area of the two (T_{ov}) i.e., $overlap(T_i^{pred}, P_j) > T_{ov} \implies MatchFound$ – hence the name overlap based tracker (OT).
- 3) If a region proposal P_j does not match any existing tracker and there are available free trackers, then a new tracker T_k is seeded and initialized with $T_k = P_j$. Every new tracker is initially set to *tracking mode* with no track count assigned to it. Once the new tracker matches one or more region proposals, it is set to *locked mode* and a track count is assigned to it.
- 4) If a T_i^{pred} matches single or multiple P_j , assign all P_j to it and update T_i and velocities as a weighted average of prediction and region proposal. Here, past history of tracker is used to remove *fragmentation* in current region proposal if multiple P_j had matched.
- 5) A P_j matching multiple T_i^{pred} , can be a result of two possible scenarios—first, due to dynamic occlusion between two moving objects and second, assignment of multiple trackers to an object resulting due to region proposals corresponding to a fragmented object in the past. An occlusion is detected if the predicted trajectory

of those trackers for $n = 2$ future time steps result in overlap. For tracker undergoing occlusion, T_i is updated entirely based on T_i^{pred} and previous velocities are retained. In the case of multiple matching trackers resulting from an earlier region proposal of a fragmented object, the multiple T_i^{pred} are merged into one tracker based on P_j and corresponding velocity is updated. The other trackers are freed up for future use.

Factoring the average probabilities of execution of logic sequences for different cases in the OT algorithm, the average number of computations per frame for OT, C_{OT} can be obtained as follows:

$$\begin{aligned}
 C_{OT} &= C_a + C_{oh} + C_u + C_{misc} \\
 C_a &= N_{obj}(19T_{locked} + 17T_{tracking} + 28P_1 + 37P_2 \\
 &\quad + 28P_3 + 37P_4 + 2P_5 + 2) \\
 C_{oh} &= N_{matched}(71 + 6P_6 + P_7) \\
 C_u &= 5T_{unmatched} \\
 C_{misc} &= 4
 \end{aligned} \tag{9}$$

where, N_{obj} is the average number of objects per frame, $N_{matched}$ is the average number of RPs matched to one or more trackers per frame, T_{locked} , $T_{tracking}$ and $T_{unmatched}$ are the average number of locked state, tracking state and unmatched trackers per frame respectively. P_1 and P_2 are the probabilities of tracker in locked state that are unmatched and matched to regions respectively, P_3 and P_4 correspond to the probabilities of tracker in tracking state that are unmatched and matched to regions respectively, P_5 is the probability of seeding a new tracker, P_6 is the probability of dynamic occlusion and P_7 is the probability of object matching multiple trackers but not involving occlusion. In equation 9, C_a , C_{oh} , C_u , C_{misc} represent the average number of computations performed per frame for assignment of RP to track, occlusion handling, handling unmatched trackers and some miscellaneous update operations, respectively. Numerical evaluation of this equation and comparison with KF will be done later in Section IV-G. The memory requirement for implementing the OT is as low as $0.5KB$ and it can be realized using registers.

D. Tracker Class Assignment

Our work in EBBIOT [13] does not have a mechanism for assigning classes to a tracker, T_i . However, with the outputs of NNDC RP acting as input to the tracker, we resolve the problem of class assignment to the detected trackers based on the following criteria:

- If the number of matched RPs to the tracker, T_i is one, assign the same class to T_i .
- Otherwise, if more than one RPs are matched to T_i , select the class with highest class confidence in the combined list of class confidences of all the matched RPs. This is the new assigned class to T_i .
- If dynamic occlusion between two tracks is detected in the frame, the class assignment is stopped for both of them and these track points are not considered for voting of class for the whole track.

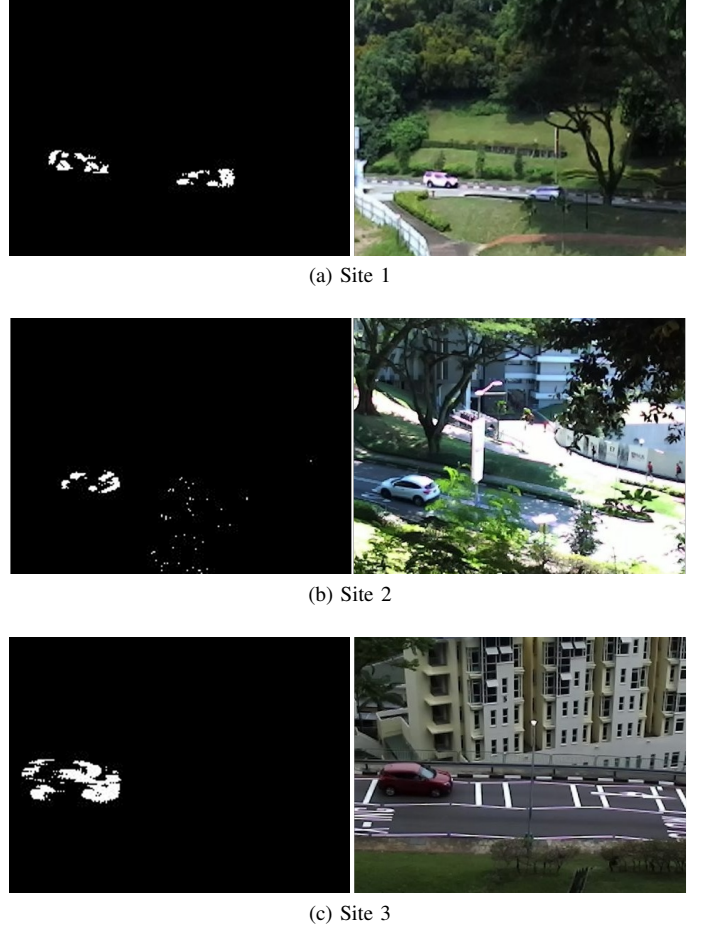


Fig. 5: Visual representation of datasets, i.e EBBI (Left) and RGB Image (Right), recorded at various sites discussed in Table II

To summarize, the event information from NVS goes into EBBI block generating 1B1C and 1B2C images. After application of median filtering on 1B1C image, it is sent to CCL RP and then, the generated RPs are further passed to NNDC block in the form of $42 \times 42 \times 2$ images containing 1B2C image of the object. The new modified RPs from NNDC are further passed to the OT for generating the trackers along with their classification. The next section will showcase the results for the described methodology.

IV. RESULTS

This section presents the data collection process followed by the evaluation of the proposed noise filtering technique. Then, we show the training of our classification model and provide insights about the hybrid RP network for the pipeline along with its comparison to other RP networks. Next, we compare the OT and KF trackers, followed by comparing the full EBBINNOT pipeline with event-based and frame-based state-of-the-art methods in Section IV-F. Finally, we compare the computations and memory usage of proposed EBBINNOT with other methods.

A. Data Acquisition

In this paper, we wanted to compare performance of NVS with a standard RGB camera; however, such a dataset is not

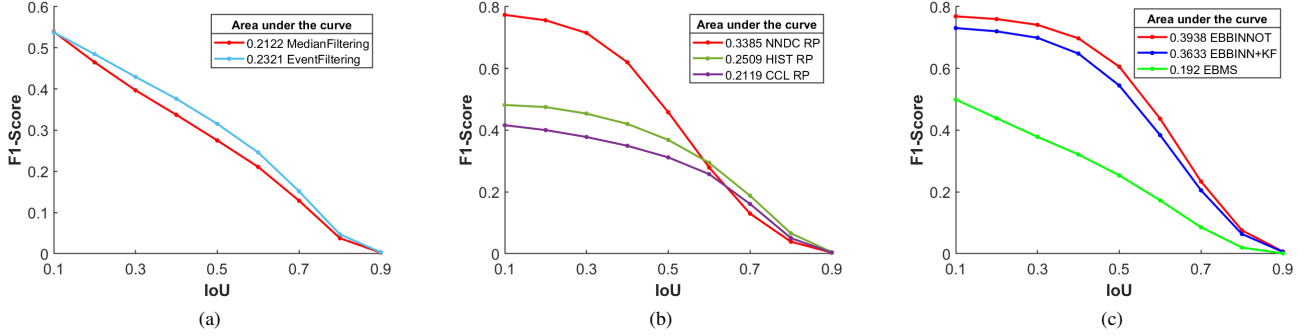


Fig. 6: (a) Comparison between Event based filtering (Refractory Filter + NN-Filter + EBBI) Vs. Median Filtering (EBBI + Median Filter) followed by CCL RP showing comparable performance with event based filtering slightly superior. (b) Comparison between different RP methods showing NNDC (CCL+NNDC) to be much superior than others in a EBBI+RP setup. (c) Comparison between trackers show EBBINNOT to be best in terms of weighted F1-Score

available as far as we know. Consequently, it demanded the acquisition of event-based data and RGB data from a real traffic scenario for training, validation and testing ¹.

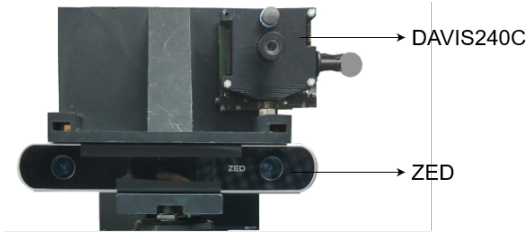


Fig. 7: Experimental setup with ZED [49] and DAVIS [14] mounted on custom-made 3D mount

The desired location for the traffic recordings was a high, perpendicular view from the road near intersections. In this regard, three places shown in Figure 5, were chosen for data collection using DAVIS. Further, we also captured RGB recordings for simultaneous comparison with the purely frame-based tracking SiamMask, as shown in Figure 7. For both the RGB and event datasets, manual ground truth (GT) annotation was carried out to facilitate tracker and classifier evaluation. In addition, the event and RGB data were made to have similar field-of-view (FoV) for a close comparison.

B. Evaluation Metrics

In order to test the system performance, we employed two evaluation metrics for object detection, classification and tracking.

- **F1 score for detection performance:** We have already discussed in Section III-B2 that IoU is an effective metric for evaluating the detection accuracy. The tracker annotation can be matched with GT annotation to get IoU in order to conclude whether it represents a true object BB ($IoU > IoU_{th}$) or a false object BB according to the threshold (IoU_{th}). Thereafter, we sweep IoU_{th} from 0.1 – 0.9 in steps of 0.1 to find out precision and recall

averaged over the entire duration of the recording. We further calculate F1 score for each recording as follows:

$$F1_{iou}^j = 2 \frac{P_{iou}^j \times R_{iou}^j}{P_{iou}^j + R_{iou}^j}$$

$$F1_{iou}^{wtd} = \frac{\sum_{j=1}^K N_{tracks}^j \times F1_{iou}^j}{\sum_{j=1}^K N_{tracks}^j} \quad (10)$$

Here, P_{iou}^j and R_{iou}^j are precision and recall for the recording j at $IoU = iou$, N_{tracks}^j represents number of tracks in recording j and $F1_{iou}^{wtd}$ represents the weighted F1 score for all the K recordings, $j = 1, \dots, K$. Thus, we examine the detection performance of our dataset in terms of $F1^{wtd}$ swept over IoU .

- **Overall accuracies for classification performance:** We calculated both the per-sample and per-track classification accuracies. In order to calculate the predicted class of a track, we recorded the statistical mode of the classification output for all the samples in the respective track of a vehicle. Further, we defined two types of accuracies: overall balanced and overall unbalanced. The former represents the average of class-wise accuracies to have a definitive evaluation measure while dealing with the dataset imbalance. The latter represents the widely used average accuracy for all the samples in the dataset regardless of class distribution.

C. Median filtered EBBI vs. Event-based noise filtering

To evaluate the effect of the proposed median filtering approach on the detection performance of the whole pipeline, we replaced it with the commonly used AER event-based nearest neighbour filtering approach [10], [50], [51]. For a fair comparison, a refractory period of $5ms$ in a neighbourhood of 3×3 was implemented for the event filtering approach, similar to the 3×3 window used for the proposed median filtering approach. Since our proposed median filter with EBBI gives on par performance with the event-based filtering approach, as shown in Figure 6(a), we advocate it for low-power hardware implementations as carried out in this work.

¹Dataset: <https://zenodo.org/record/3839231>

TABLE II: DAVIS traffic dataset

Recording Site	Duration	Time of Day	Lens Resolution	Number of Events	# of Recordings		Car/Van		Bus		Bike		Truck	
					in Training	Testing	(Samples Tracks)	(Samples Tracks)	(Samples Tracks)	(Samples Tracks)				
Site 1	2h11m	3PM, 4PM	12mm	201M	6	2	18232 379	8081 165	1378 35	2256 47				
Site 2	2h25m	3PM, 4PM	6mm	132M	6	3	16918 382	8019 177	1604 39	2513 56				
Site 3	1h	3PM	8mm	50M	2	1	6514 209	1201 27	512 22	501 15				

TABLE III: Mean object sizes at different recording sites

Recording Site	Car/Van	Bus	Bike	Truck
Site 1	16 × 42	31 × 94	15 × 21	22 × 50
Site 2	25 × 47	52 × 107	17 × 22	35 × 61
Site 3	34 × 82	64 × 180	26 × 44	50 × 104

D. Comparison of Region Proposal Networks

Data Preparation for NNDC training: As mentioned in Section III-A1, events were aggregated at a frame rate of 15 Hz ($t_F = 66$ ms) to form 1B1C and 1B2C frames. We noted that the size of objects played a significant role for the NNDC model since an anchor box guides the class size. The objects at site 3 location had significantly different mean class sizes when compared to other sites (shown in Table III). Therefore, to facilitate the model training, we rescaled the frame by half to 120×90 at site 3 location using nearest neighbor interpolation.

Table II shows the statistical distribution of the dataset in terms of the number of samples obtained for each class category, and the number of recordings kept from each site for training and testing. The $42 \times 42 \times 2$ samples from the frames are obtained after applying CCL RP along with their correct positions, BB_{conf} and class information, by matching the respective samples with interpolated GT annotations. We also randomly selected $\approx 63,000$ noisy samples obtained from CCL RP that did not match with any GT annotations (with $IoU < 0.1$) so that the network could classify them as a separate background class and give a predicted \hat{BB}_{conf} to each less than $thr = 0.1$. Assigning a different class was also necessary because these samples do not fit in any class category and in this class’s absence, $Loss_1$ could not be optimized.

Note that we did not consider samples from pedestrians in the training data acquisition since they generate very few events due to their small size and slow speed. Simultaneous tracking of pedestrians and vehicles is kept as a future work. In total, we had $C = 5$ with classes: background, car/van, bus, bike and truck in our model with a total of $C + 5 = 10$ outputs. Since the buses and trucks were generally bigger than the size of 42×42 , we also included cropped samples from top-left, top-right, bottom-left and bottom-right sections of their RPs. This helped to reduce the class-wise sample variance, and also provided the information from the object’s frontal and posterior region for tuned BB prediction. The bikes were augmented by random rotation within ± 15 and translation by some random amounts within the fixed area of 42×42 . The samples from recordings assigned for testing were also collected using the same criteria, but without any noisy samples having an $IoU < 0.1$. The main objective of the training was to improve the BB_{conf} , increase the BB actual overlap with the object, and also report its correct class.

Training Details: NNDC model was trained on 80% of the training data randomly selected, while the rest was kept for validation. The model was trained on an NVIDIA TITANX GPU in the form of randomly shuffled batches of 128 with 20 assigned epochs, a learning rate of 0.01 and $\lambda = 5$. This model, trained using Adam optimizer with default hyperparameters, was written in Keras framework because of the ease of writing custom loss functions like equation 8. Further, the overall unbalanced accuracy metrics on validation data after each epoch were used for early stopping of the training with patience 3. The best model was saved for evaluation on the test recordings collected at different times.

TABLE IV: Classification accuracies for testing samples recorded using DAVIS

Category	per sample (%)	per track (%)
Car/Van	86.59	95.8
Bus	89.81	98.1
Bike	81.02	100
Truck	53.39	76.92
Unbalanced accuracy	85.07	95.39
Balanced accuracy	77.70	92.70

Inference: Table IV shows the per-sample as well as per-track accuracies on all the test recordings, including overall balanced and unbalanced accuracies. As expected, per track accuracies are higher due to the majority voting, and in the case of the Bike category, it is possible to get 100% classification performance. We attribute this to the unique size and shape of the bikes relative to the other categories. Overall, the balanced accuracy closely trails the unbalanced accuracy, which implies the classifier makes sound judgements instead of skewed decisions caused by the unbalanced DAVIS dataset.

Overall RP Comparison: In order to pick the best region proposal for the proposed pipeline, we ran the three RPNs, namely HIST, CCL and CCL + NNDC RP on the test dataset while restricting the maximum RPs to eight per frame. In this evaluation, the greedy NMS in NNDC had $thr^{n.s} = 0.3$ for suppressing the boxes. To compare the performance at different $IoUs$, we used ground truth annotations at the same timestamps corresponding to the RPs.

Figure 6(b) shows the weighted F1 scores for the different RPs. Overall, the proposed CCL+NNDC RP significantly outperforms other RPs, as shown in Figure 6(b) with higher area under curve (AUC), calculated using trapezoidal numerical integration. Interestingly, HIST RP performs better than CCL RP by itself, due to lesser fragmentation by merging of overlapping regions. Integrating NNDC after CCL significantly improves this performance. Therefore, we adapt CCL+NNDC RP as part of our proposed pipeline and is also referred as hybrid RP.

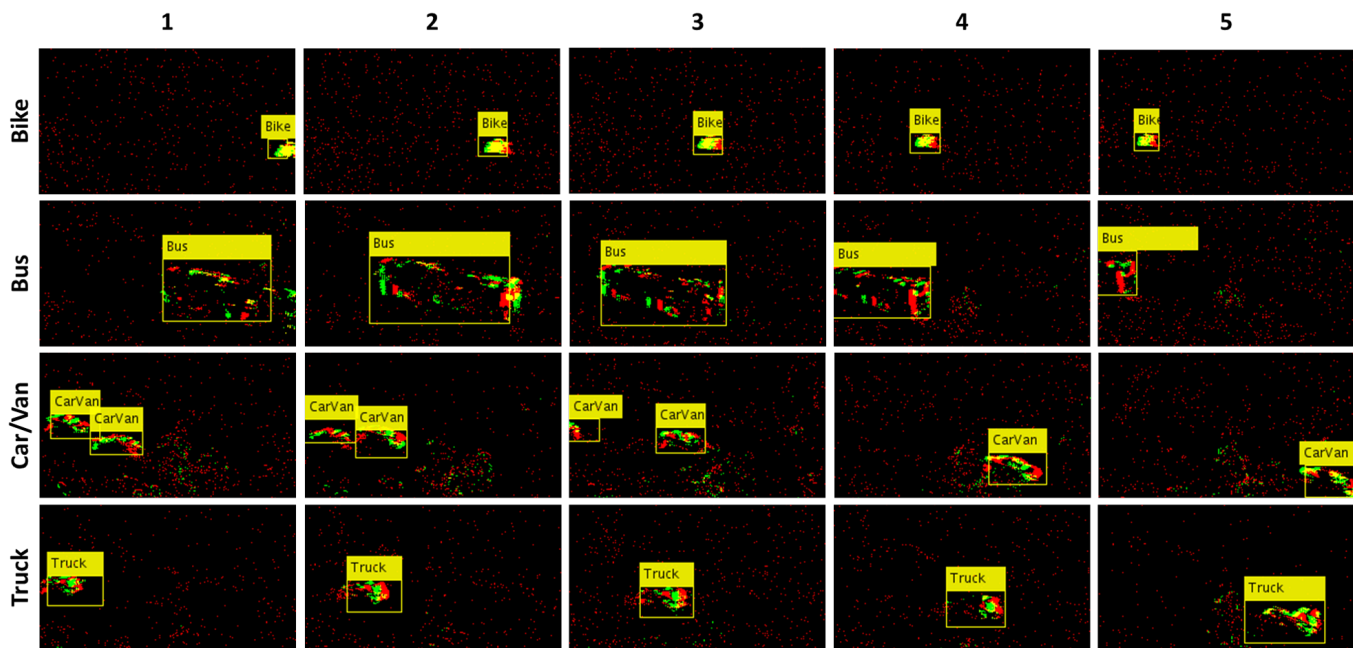


Fig. 8: Exemplar detection and classification results from the described EBBINNOT pipeline for tracks of different vehicles

E. Comparison of Tracker

For the purpose of fair comparison of performance of different trackers, we ensured that the same region proposal network, tracker parameters, tracker log generation method and evaluation metrics were used. For comparison of KF-Tracker and OT, the number of region proposals and trackers per frame were restricted to a maximum of 8, the threshold for treating an object to be lost during tracking was set at invisibility for 5 consecutive frames or less than 60% visibility when the track is still valid. While for EBMS, the events were filtered using a refractory layer with period of $50ms$, followed by NN-Filter with period of $5ms$. The minimum number of events required for cluster formation were kept 8, maximum radius of cluster was kept 130, and a time limit of $100ms$ was assigned in case of inactivity of cluster. These hyperparameter values were obtained after series of runs for optimization of EBMS. Figure 8 illustrates the sample tracks generated for different types of vehicles for the trained EBBINNOT pipeline. Based on the observations made in [38], we excluded tracks for human class while calculating the F1-scores for all the 5 test dataset recordings excluding site 3.

As shown in Figure 6(c), it can be noted that OT performs slightly better than KF and significantly better than the purely event based EBMS tracker. In order to ascertain the reason for performance improvement in OT as compared to KF, we performed an ablation study by removing specific parts of heuristics used in OT. Based on these comparisons, we can attribute the enhanced performance of OT to two reasons: first, the presence of a *tracking* mode before transitioning to *locked* state and second, the fragmentation handling logic in the OT. In our algorithm, only trackers in the *locked* state are considered as a valid track. In the KF tracker with no *tracking* mode, we observed that noisy event occurring intermittently results in false RPs creating new tracks for each of these noisy

objects and increasing the false positives. As for fragmentation handling, unlike KF which cannot handle multiple trackers resulting from a fragmented object, OT utilizes past history of trackers to resolve a fragmentation in case multiple RPs match a tracker and merges multiple trackers that might be corresponding to an earlier fragmented RP, following the steps listed in Section III-C. This logic effectively reduces multiple tracks being assigned to the same object and thereby boosts the performance of OT.

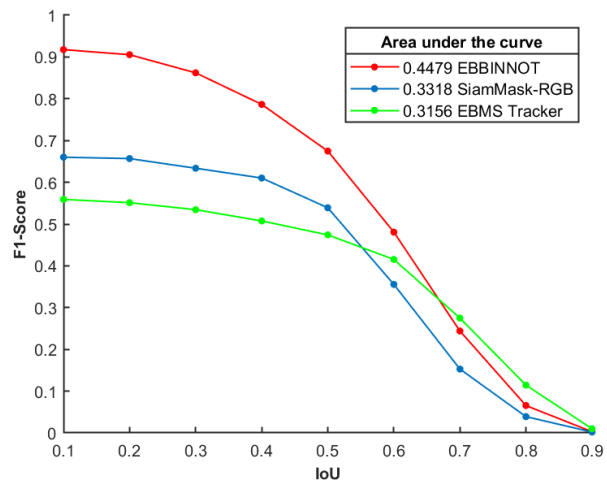
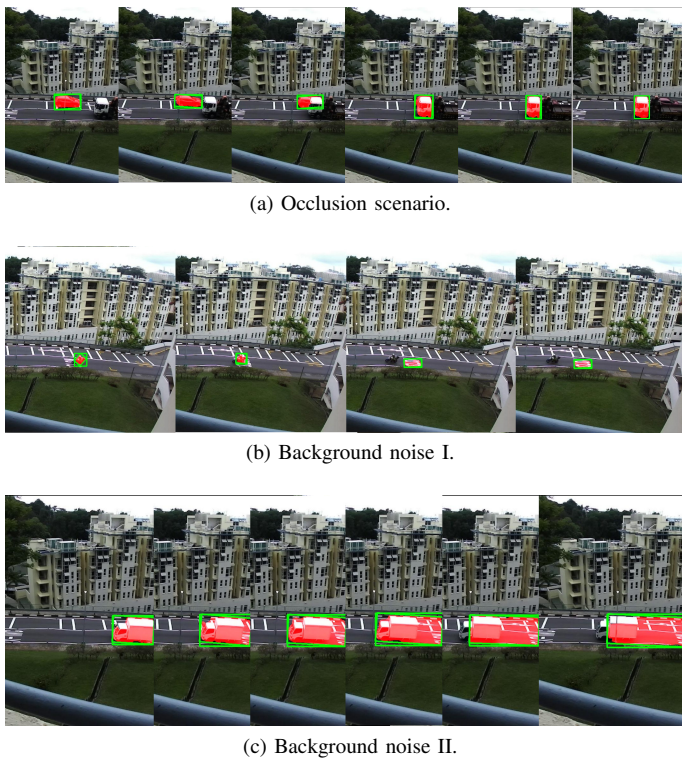


Fig. 9: Comparison of the proposed EBBINNOT, SiamMask [28] and Event-Based Mean-Shift (EBMS) [7]

F. Comparison to state-of-the-art

In this section, we report the performance of the proposed EBBINNOT compared to the frame-based state-of-the-art tracker, namely SiamMask, and event-based state-of-the-art approach EBMS. Since $2/3^d$ of data recorded at site 3



(a) Occlusion scenario.

(b) Background noise I.

(c) Background noise II.

Fig. 10: Tracking performance of SiamMask under challenging scenarios. It fails to track either to background road markings or occluding objects becoming part of its online object learning representation

was used to train NNDC model, as stated in Table II, we used remaining $1/3^{rd}$ of data for evaluation. Note that original RGB dataset with FoV 90° is used as input to SiamMask and corresponding output is referred as SiamMask-RGB in this section.

Figure 9 shows the F1 scores at various IoU_{th} for test recording at site 3. We observed that SiamMask was not able to match the performance of EBBINNOT due to its inherent use of similarity matching, which failed under occlusion scenarios. In other words, SiamMask fails to perform in scenarios where vehicles pass each other, as illustrated in Figure 10a. The other factor contributing to SiamMask’s poor performance was that the background road markings and footpath patterns of the scene became part of the object representation as shown in Figure 10b, causing missed tracks.

Overall, our proposed tracker outperforms the multi-object EBMS tracker and SiamMask. In spite of this good performance, it was noticed that on re-scaling the frame size by half to 120×90 at site 3 location, as previously noted in Section IV-D, the NNDC model did not always pick the right size for individual classes. This minor drawback remains to be addressed in future works using techniques such as transfer learning.

G. Computational Cost

The average number of computations per frame performed by KF-Tracker (C_{KF}) and OT (C_{OT}) were estimated using eq. 1 and eq. 9 respectively, and these results were verified to be close to the actual computation count obtained by

TABLE V: Computational Count Estimation: C_{KF} Vs. C_{OT}

Recording Site	No. of Recordings	OT Estimate	KF Estimate	KF:OT
Site 1	4	119	698	6
Site 2	4	351	2472	7
Average	8 Recordings	235	1585	6.5

incrementing a counter with count weighted by computations in a step at run time, with an error margin of $\pm 0.01\%$. As shown tabulated in Table V, KF-Tracker performs $\approx 6.5\times$ more computations averaged across 8 recordings at 2 sites as compared to the OT.

Based on the SiamMask architecture presented in [28], computations and memory usage are calculated layer-by-layer and then summed considering all network parameters and input dimensions. Total computations and memory requirements were deduced to be $\approx 38000M$ operations per frame and $\approx 157MB$ respectively.

It is already known from Section III-B2 that EBBINN has a computes bound of $\approx 17.3M$ operations per frame and since OT does not add much computes, SiamMask uses $\approx 2200\times$ more computes per frame and demands $\approx 1450\times$ more memory than EBBINNOT, due to its Siamese-based deep neural network architecture. Therefore, EBBINNOT offers a fair advantage in terms of total computation and memory usage.

The total number of computes per frame (C_{EBMS}) and the memory requirement in bits (M_{EBMS}) for the EBMS [13] algorithm are given by,

$$\begin{aligned} C_{EBMS} &= \bar{N} \times [9 \overline{CL}^2 + (169 + 16 \gamma_{merge}) \overline{CL} + 11] \\ M_{EBMS} &= 408CL_{max} + 56 \end{aligned} \quad (11)$$

respectively, where \bar{N} is the average number of events per frame, \overline{CL} is the average number of active clusters at any given time ($\approx \bar{N}_T$), γ_{merge} is the probability of two clusters merging, and CL_{max} is the maximum number of potential clusters. Assuming the past 10 positions of cluster for the current velocity calculation, $CL_{max} = 8$ and for our dataset, $\overline{CL} \approx 2$, $\gamma_{merge} \approx 0.1$ and $\bar{N} \approx 650$, EBMS requires 252 kops per frame which is $\approx 68\times$ lower than EBBINNOT, and a memory of 3.32KB, which is nearly negligible.

The proposed EBBINNOT, however, significantly outperforms EBMS as shown in Figures 6(c) & 9. This performance gain comes at the cost of slightly higher computations and memory usage. Overall, out of the three approaches considered here, EBBINNOT offers the best trade off between performance and computational complexity.

V. DISCUSSION

A. Repeatability of results for recordings with other NVS - CeleX

The proposed flow consisting EBBI creation, median filtering, NNDC and OT was also verified for repeatability on recordings from the CeleX [15] camera. We collected a total of 35 recordings at different times from a single location and divided them in the ratio of 5:2 for training and testing. After reviewing the size distribution of the objects from different classes obtained from the GT annotations and comparing it

TABLE VI: Classification Scores for testing videos recorded on CeLeX

Category	per sample (%)	per track (%)
Car/Van	93.38	95.61
Bus	96.4	95.65
Bike	89.38	96.3
Truck	50.57	80
Unbalanced accuracy	91.64	95.27
Balanced accuracy	82.43	91.89

with the distribution from earlier recordings, we settled to resize the images by a factor of 3.33 to 384×240 from 1280×800 .

Due to the camera’s invalid polarity output at some points, only 1B1C images were stored for training the NNDC model. Thus, during training and testing, the RP input to NNDC had a size of $42 \times 42 \times 1$ and the output BB coordinates were also scaled according to the new image size. We balanced the training data by augmentation and further removed the excess number of examples in classes like cars because they often appeared in the field of view.

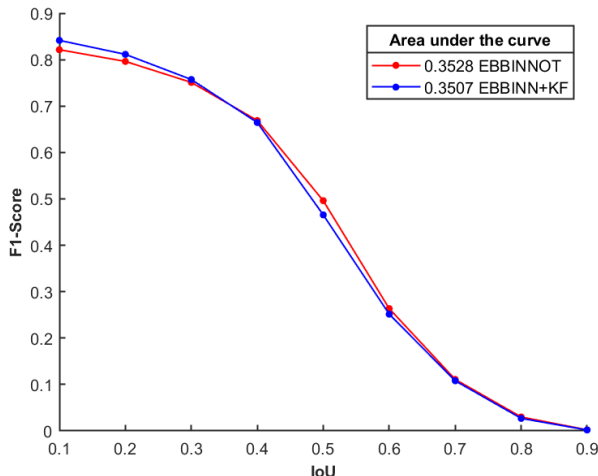
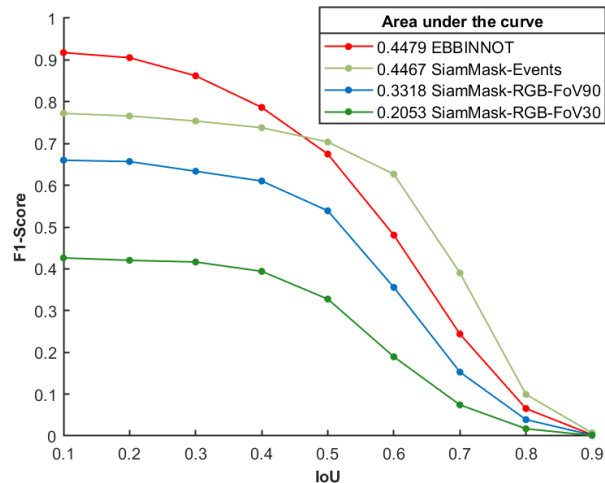


Fig. 11: Weighted F1 scores for CeleX recordings showing similar performance to the DAVIS recordings

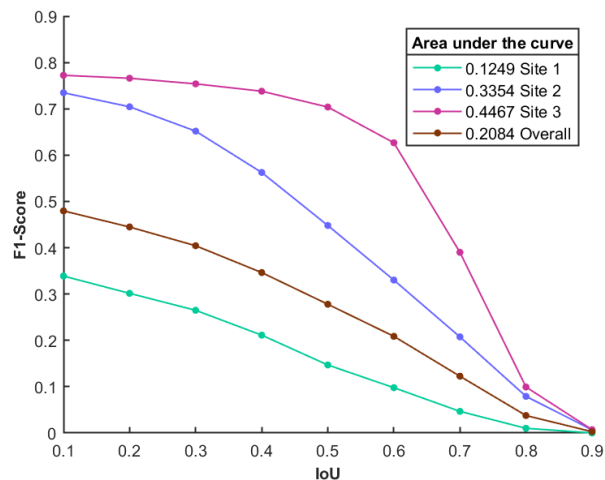
The model was trained on the same configurations explained in Section IV-D and the best model yielded the classification results shown in Table VI. Moreover, the detection performance was checked after running the actual 10 testing videos on the entire setup and the generated annotations were rescaled back to the original sensor dimensions by multiplication with 3.33. We calculated the weighted F1 scores shown in Figure 11, and as expected, the performance for these recordings are comparable to the performance results of the proposed flow for DAVIS recordings, thus proving repeatability and reproducibility of the results for different recordings from different neuromorphic vision sensors.

B. Analyzing SiamMask with Events vs. RGB data

In order to investigate whether the major improvement in performance of EBBINNOT comes from the background rejection property of NVS, we applied the SiamMask tracker on the EBBI directly and evaluated its performance compared



(a)



(b)

Fig. 12: (a) F1 scores of SiamMask on Event and RGB data for site 3. (b) Weighted F1 scores of SiamMask-Events for different site recordings

to SiamMask-RGB and EBBINNOT. The results obtained with EBBI as the input to SiamMask are hereby referred to as SiamMask-Events. Moreover, the DAVIS recordings are of FoV 31° , whereas the RGB dataset has FoV 90° , which makes the comparison with SiamMask-Events harder in terms of track length. To alleviate this, the RGB dataset with FoV 90° is further processed to generate another RGB dataset with FoV restricted to 30° . The results obtained using the RGB dataset with FoV 30° and FoV 90° as inputs to SiamMask are hereby referred as SiamMask-RGB-FoV30 and SiamMask-RGB-FoV90 respectively (the visual representation of EBBI and RGB image with FoV 30° is shown in Figure 5).

Figure 12(a) shows F1 scores at different IoU_{th} corresponding to EBBINNOT, SiamMask-Events, SiamMask-RGB-FoV90, and SiamMask-RGB-FoV30 for site 3 test recordings. At lower IoU_{th} , EBBINNOT outperforms SiamMask-Events and vice versa for higher IoU_{th} . It can be seen that SiamMask-Events perform better than SiamMask-RGB due to the following reasons: (a) input to the SiamMask-Events has less background information (noise) and robustness towards

motion blur. (b) the road markings during initialization of the object when it enters the scene caused missed tracks, as they became part of the object representation and severely affected SiamMask-RGB-FoV30 performance. The latter was also the main reason for poor performance of SiamMask-RGB-FoV30 compared to SiamMask-RGB-FoV90, as the markings were further away in the wider field-of-view recording.

From Figure 12(b), it can be observed that size of classes at each site location is proportional to SiamMask-Events' performance. In other words for larger object size, SiamMask naturally performs better with clearer visual information. The size distribution of various objects at different sites is shown in Table III. At site 3, objects are fairly larger in size compared to the other site recordings, and thus it was chosen as final comparative evaluation for SiamMask-Events in Figure 12(a). It is clear when SiamMask-Events is applied for all site recordings, overall performance is $2\times$ lower compared to EBBINOT in terms of area under the curve. In summary, EBBINOT is better compared to the deep learning based SiamMask in terms of applicability and performance when evaluated on all locations, while enabling efficient hardware implementation.

VI. CONCLUSION

This paper proposes a new hybrid event-frame pipeline called EBBINNOT for the IoT based traffic monitoring system using a stationary NVS. EBBINNOT creates an event based binary image and after median filtering it, sends it to connected component labelling based region proposal network and then to NNDC for merging fragmented proposals, predicting their correct sizes and class categories. The modified proposals are then passed to an overlap based tracker having tracking/locked state trackers, heuristics for handling occlusion and other simplified methods inspired from Kalman Filter. All the mentioned blocks in EBBINNOT are completely optimized for computational costs. EBBINNOT requires $\approx 17.3M$ operations per frame, almost $2200\times$ less than the state-of-the-art purely frame-based SiamMask tracker and even outperforms it in tracking performance by AUC of ≈ 0.12 calculated on the simultaneously collected events and RGB data. Further, this system also shows a substantial improvement from the purely events-based approach called EBMS with tracking performance difference of AUC ≈ 0.14 , though requiring $\approx 68\times$ more computations. EBBINNOT also achieves an overall balanced track accuracy of 92.70% on recordings from three sites spanning more than five hours.

Moreover, we show that individual blocks of EBBINNOT perform better than the corresponding traditional algorithms. The proposed hybrid RPN-CCL combined with NNDC-performs better (AUC = 0.34) than other object detection methods (AUC < 0.25) for event-data; it requires $\approx 17.3M$ computes which is $< 16\times$ the computations needed by other neural network based detectors and classifiers. Further, we show that OT generates tracking results with AUC = 0.39, and just about one-sixth of computes as compared to KF tracker which also has poorer performance (AUC = 0.36).

REFERENCES

- [1] C. Posch, T. Serrano-Gotarredona, B. Linares-Barranco, and T. Delbruck, "Retinomorphonic Event-Based Vision Sensors: Bioinspired Cameras With Spiking Output," *Proceedings of the IEEE*, vol. 102, no. 10, pp. 1470–1484, 2014.
- [2] A. Basu, *et al.*, "Low-power, adaptive neuromorphic systems: Recent progress and future directions," *IEEE Journal on Emerging and Selected Topics in Circuits and Systems*, vol. 8, no. 1, pp. 6–27, 2018.
- [3] G. Gallego, *et al.*, "Event-based Vision: A Survey," *CoRR*, vol. abs/1904.08405, 2019.
- [4] Z. Ni, C. Pacoret, R. Benosman, S. Ieng, and S. RÉGNIER*, "Asynchronous event-based high speed vision for microparticle tracking," *Journal of microscopy*, vol. 245, no. 3, pp. 236–244, 2012.
- [5] H. Liu, *et al.*, "Combined frame-and event-based detection and tracking," in *2016 IEEE International Symposium on Circuits and Systems (ISCAS)*. IEEE, 2016, pp. 2511–2514.
- [6] L. A. Camuñas-Mesa, T. Serrano-Gotarredona, S.-H. Ieng, R. Benosman, and B. Linares-Barranco, "Event-driven stereo visual tracking algorithm to solve object occlusion," *IEEE transactions on neural networks and learning systems*, vol. 29, no. 9, pp. 4223–4237, 2017.
- [7] T. Delbruck and M. Lang, "Robotic goalie with 3 ms reaction time at 4% CPU load using event-based dynamic vision sensor," *Frontiers in neuroscience*, vol. 7, p. 223, 2013.
- [8] B. Ramesh, *et al.*, "Long-term object tracking with a moving event camera," in *BMVC*, 2018, p. 241.
- [9] J. Redmon and A. Farhadi, "YOLOv3: An Incremental Improvement," 2018.
- [10] V. Padala, A. Basu, and G. Orchard, "A Noise Filtering Algorithm for Event-Based Asynchronous Change Detection Image Sensors on TrueNorth and Its Implementation on TrueNorth," *Frontiers in Neuroscience*, vol. 12, p. 118, 2018.
- [11] A. Sironi, M. Brambilla, N. Bourdis, X. Lagorce, and R. Benosman, "HATS: Histograms of Averaged Time Surfaces for Robust Event-based Object Classification," 2018.
- [12] J. Pei, *et al.*, "Towards artificial general intelligence with hybrid Tianjic chip architecture," *Nature*, vol. 572, no. 7767, pp. 106–111, 2019.
- [13] J. Acharya, *et al.*, "EBBIOT: A Low-complexity Tracking Algorithm for Surveillance in IoT Using Stationary Neuromorphic Vision Sensors," *arXiv preprint arXiv:1910.01851*, 2019.
- [14] C. Brandli, R. Berner, M. Yang, S.-C. Liu, and T. Delbruck, "A 240×180 130 db 3 μ s latency global shutter spatiotemporal vision sensor," *IEEE Journal of Solid-State Circuits*, vol. 49, no. 10, pp. 2333–2341, 2014.
- [15] M. Guo, J. Huang, and S. Chen, "Live demonstration: A 768×640 pixels 200Meps dynamic vision sensor," in *2017 IEEE International Symposium on Circuits and Systems (ISCAS)*. IEEE, 2017, pp. 1–1.
- [16] C. Brandli, *et al.*, "Live demonstration: The "DAVIS" Dynamic and Active-Pixel Vision Sensor," in *2014 IEEE International Symposium on Circuits and Systems (ISCAS)*. IEEE, 2014, pp. 440–440.
- [17] H. Yang and *et al.*, "Recent advances and trends in visual tracking: A review," *Neurocomputing*, vol. 74, pp. 3823–31, 2011.
- [18] J. Acharya, *et al.*, "A Comparison of Low-complexity Real-Time Feature Extraction for Neuromorphic Speech Recognition," *Frontiers in Neuroscience*, vol. 12, p. 160, 2018.
- [19] L. A. Camuñas-Mesa, T. Serrano-Gotarredona, S. Ieng, R. Benosman, and B. Linares-Barranco, "Event-Driven Stereo Visual Tracking Algorithm to Solve Object Occlusion," *IEEE Transactions on Neural Networks and Learning Systems*, vol. 29, no. 9, pp. 4223–4237, 2018.
- [20] L. Lin, B. Ramesh, and C. Xiang, "Biologically Inspired Composite Vision System for Multiple Depth-of-field Vehicle Tracking and Speed Detection," in *Computer Vision - ACCV 2014 Workshops*. Springer International Publishing, 2015, pp. 473–486.
- [21] A. Valade, P. Acco, P. Grabolosa, and J.-Y. Fourniols, "A Study about Kalman Filters Applied to Embedded Sensors," *Sensors (Basel, Switzerland)*, vol. 17, 2017.
- [22] J. R. Munkres, "Algorithms for the Assignment and Transportation Problems," *Journal of the Society for Industrial and Applied Mathematics*, vol. 5, pp. 32–38, 1957.
- [23] M. Page, "Microprocessor implementation of the kalman filter," *Microelectronics Journal*, vol. 10, no. 3, pp. 16–22, 1979.
- [24] D. Comaniciu and V. Ramesh, "Mean shift and optimal prediction for efficient object tracking," in *Proceedings 2000 International Conference on Image Processing (Cat. No. 00CH37101)*, vol. 3. IEEE, 2000, pp. 70–73.
- [25] J. Bromley, I. Guyon, Y. LeCun, E. Säckinger, and R. Shah, "Signature verification using a "siamese" time delay neural network," in *Advances in neural information processing systems*, 1994, pp. 737–744.

- [26] G. R. Koch, "Siamese Neural Networks for One-Shot Image Recognition," 2015.
- [27] L. Bertinetto, J. Valmadre, J. F. Henriques, A. Vedaldi, and P. H. S. Torr, "Fully-Convolutional Siamese Networks for Object Tracking," *CoRR*, vol. abs/1606.09549, 2016.
- [28] Q. Wang, L. Zhang, L. Bertinetto, W. Hu, and P. H. Torr, "Fast online object tracking and segmentation: A unifying approach," in *Proceedings of the IEEE Conference on Computer Vision and Pattern Recognition*, 2019, pp. 1328–1338.
- [29] G. Cohen, *et al.*, "Spatial and temporal downsampling in event-based visual classification," *IEEE Trans. on Neural Networks and Learning Systems*, vol. 29, no. 10, pp. 5030–44, 2018.
- [30] D. Singla, *et al.*, "HyNNA: Improved Performance for Neuromorphic Vision Sensor based Surveillance using Hybrid Neural Network Architecture," 2020.
- [31] R. C. Gonzalez and R. E. Woods, *Digital Image Processing (3rd Edition)*. Upper Saddle River, N.J.: Prentice Hall, 2008.
- [32] P. A. Merolla, *et al.*, "A million spiking-neuron integrated circuit with a scalable communication network and interface," *Science*, vol. 345, no. 6197, pp. 668–673, 2014.
- [33] I. Lungu, F. Corradi, and T. Delbrück, "Live demonstration: Convolutional neural network driven by dynamic vision sensor playing RoShamBo," in *2017 IEEE International Symposium on Circuits and Systems (ISCAS)*, 2017, pp. 1–1.
- [34] D. Czech and G. Orchard, "Evaluating noise filtering for event-based asynchronous change detection image sensors," in *IEEE/RAS-EMBS International Conference on Biomedical Robotics and Biomechatronics (BioRob)*. IEEE, 2016.
- [35] R. Veale, Z. M. Hafed, and M. Yoshida, "How is visual salience computed in the brain? Insights from behaviour, neurobiology and modelling," *Philosophical Transactions of the Royal Society B: Biological Sciences*, vol. 372, no. 1714, p. 20160113, 2017.
- [36] B. J. White, J. Y. Kan, R. Levy, L. Itti, and D. P. Munoz, "Superior colliculus encodes visual saliency before the primary visual cortex," *Proceedings of the National Academy of Sciences*, vol. 114, no. 35, pp. 9451–9456, 2017.
- [37] S. Yohanandan, A. Song, A. G. Dyer, and D. Tao, "Saliency preservation in low-resolution grayscale images," in *Proceedings of the European Conference on Computer Vision (ECCV)*, 2018, pp. 235–251.
- [38] A. Ussa, *et al.*, "A low-power end-to-end hybrid neuromorphic framework for surveillance applications," vol. abs/1910.09806, 2019.
- [39] S. Afshar, T. J. Hamilton, J. Tapsos, A. V. Schaik, and G. Cohen, "Investigation of Event-Based Surfaces for High-Speed Detection, Unsupervised Feature Extraction, and Object Recognition," *Frontiers in Neuroscience*, vol. 12, p. 1047, 2019.
- [40] L. He, *et al.*, "The connected-component labeling problem: A review of state-of-the-art algorithms," *Pattern Recognition*, vol. 70, pp. 25–43, 2017.
- [41] R. Walczyk, A. Armitage, and T. D. Binnie, "Comparative study on connected component labeling algorithms for embedded video processing systems," *IPCV*, vol. 10, p. 176, 2010.
- [42] J. Redmon and A. Farhadi, "YOLO9000: Better, Faster, Stronger," 2016.
- [43] W. Liu, *et al.*, "SSD: Single Shot MultiBox Detector," *Lecture Notes in Computer Science*, p. 21–37, 2016.
- [44] Y. LeCun, *et al.*, "Comparison of learning algorithms for handwritten digit recognition," in *International conference on artificial neural networks*, vol. 60. Perth, Australia, 1995, pp. 53–60.
- [45] Y. LeCun, L. Bottou, Y. Bengio, P. Haffner, *et al.*, "Gradient-based learning applied to document recognition," *Proceedings of the IEEE*, vol. 86, no. 11, pp. 2278–2324, 1998.
- [46] J. Redmon, S. Divvala, R. Girshick, and A. Farhadi, "You Only Look Once: Unified, Real-Time Object Detection," 2015.
- [47] J. Hosang, R. Benenson, and B. Schiele, "Learning non-maximum suppression," 2017.
- [48] J. Pedoem and R. Huang, "YOLO-LITE: A Real-Time Object Detection Algorithm Optimized for Non-GPU Computers," 2018.
- [49] "Stereo Labs," <https://www.stereolabs.com/zed/>, accessed: 2020-03-27.
- [50] B. Ramesh, A. Ussa, L. Della Vedova, H. Yang, and G. Orchard, "Low-Power Dynamic Object Detection and Classification With Freely Moving Event Cameras," *Frontiers in Neuroscience*, vol. 14, p. 135, 2020.
- [51] B. Ramesh, H. Yang, G. Orchard, N. Thi, and C. Xiang, "DART: Distribution Aware Retinal Transform for Event-based Cameras," *IEEE Transactions on Pattern Analysis and Machine Intelligence*, pp. 1–1, 2019.

Deepak Singla (M' 20) received his B.Tech in Electrical Engineering (Power & Automation) from the Indian Institute of Technology, Delhi in 2018. After the graduation, he joined Nanyang Technological University, Singapore as a Project Officer in the BRAIN Systems Lab - CICS headed by Dr. Basu. Since then, he is working on IoT based applications of neuromorphic vision sensors and designing low computational cost and reliable systems for the same. His research interests include neuromorphic engineering, brain-machine intelligence and computer vision.

Vivek Mohan (S' 14) received his B.Tech. degree in Electronics and Communication Engineering from JNTU - Hyderabad in 2016 and Joint M.Sc. in Integrated Circuit Design from Technical University of München and Nanyang Technological University (NTU) Singapore in 2019. After graduation, he worked as a Research Associate in the BRAIN Systems Lab - CICS, NTU in the area of neuromorphic vision. Vivek is currently a Ph.D. candidate at the School of Electrical and Electronic Engineering, NTU. His research interests include integrated circuit design, neuromorphic engineering, signal processing, and is currently focused on intra-cortical brain-machine interface.

Tarun Pulluri received his B.Tech degree in Electronics and Communications Engineering from JNTUH College of Engineering Hyderabad and Master of Engineering degree in Microelectronics and Embedded Systems from Asian Institute of Technology in 2018. After graduation, he joined AIT as a Research Associate in the AI Center and was working on deep learning and computer vision applications. He is currently working as a Research Attachment in the Neuromorphic lab at the National University of Singapore. His research interests include computer vision, deep learning, neuromorphic engineering, and robotics.

Andres Ussa received his B.Sc. degree in Mechatronics Engineering from Nueva Granada Military University in 2012 and Joint M.Sc. in Embedded Computing Systems from TU Kaiserslautern and University of Southampton in 2016. His previous research experience has been focused on embedded systems design and machine learning applications. He had a short experience as a Software/Hardware Developer for consumer electronics.

Bharath Ramesh received the B.E. degree in Electrical & Electronics Engineering from Anna University of India in 2009; M.Sc. and Ph.D. degrees in Electrical Engineering from National University of Singapore in 2011 and 2015 respectively, working at the Control and Simulation Laboratory on Image Classification using Invariant Features. Bharath's main research interests include pattern recognition and computer vision. At present, his research is centered on event-based cameras for autonomous robot navigation.

Arindam Basu (M' 10, SM' 17) received the B.Tech and M.Tech degrees in Electronics and Electrical Communication Engineering from the Indian Institute of Technology, Kharagpur in 2005, the M.S. degree in Mathematics and Ph.D. degree in Electrical Engineering from the Georgia Institute of Technology, Atlanta in 2009 and 2010 respectively. Dr. Basu received the Prime Minister of India Gold Medal in 2005 from I.I.T Kharagpur. He joined Nanyang Technological University in June 2010 and currently holds a tenured Associate Professor position.

He is currently an Associate Editor of IEEE Sensors journal, IEEE Transactions on Biomedical Circuits and Systems and Frontiers in Neuroscience. He was a Distinguished Lecturer for IEEE Circuits and Systems Society for the 2016-17 term. Dr. Basu received the best student paper award at Ultrasonics symposium, 2006, best live demonstration at ISCAS 2010 and a finalist position in the best student paper contest at ISCAS 2008. He was awarded MIT Technology Review's inaugural TR35@Singapore award in 2012 for being among the top 12 innovators under the age of 35 in SE Asia, Australia and New Zealand. His research interests include bio-inspired neuromorphic circuits, non-linear dynamics in neural systems, low power analog IC design and programmable circuits and devices.